



ANNUAL REPORT 2016

Frank Laboratory of Neutron Physics

V.N. Shvetsov, D.M. Chudoba

Dubna 2016

In 2016, the Frank Laboratory of Neutron Physics scientific programme was aimed at obtaining new results under four research themes of the JINR Plan for Scientific Research and International Scientific and Technical Cooperation: in condensed matter physics ("Investigations of Condensed Matter by Modern Neutron Scattering Methods", 04-4-1121-2015/2017, headed by D.P. Kozlenko, V.L. Aksenov and A.M. Balagurov; "Multimodal Platform for Raman and Nonlinear Optical Microscopy and Microspectroscopy for Condensed Matter Studies", 04-4-1111-2013/2017 headed by G.M. Arzumanyan); in neutron nuclear physics ("Investigations in the Field of Nuclear Physics with Neutrons", 03-4-1104-2011/2016, headed by V.N. Shvetsov, Yu. N. Kopatch, E.V. Lychagin, and P.V. Sedyshev); in development of the FLNP basic facilities ("Development of the IBR-2 Facility with a Complex of Cryogenic Neutron Moderators", 04-4-1105-2011/2016, headed by A.V. Belushkin and A.V. Vinogradov); in development of the IBR-2 spectrometers and computation complex ("Development of Experimental Facilities for Condensed Matter Investigations with Beams of the IBR-2 Facility", 04-4-1122-2015/2017, headed by S.A. Kulikov and V.I. Prikhodko).

1. CONDENSED MATTER PHYSICS

The greater part of experimental research was carried out on the spectrometers of the modernized IBR-2 reactor.

In 2016, within the framework of the User Programme 238 proposals for conducting experiments were received from 19 different countries. The received proposals covered the broad spectrum of neutron research in physics (30%), materials science (35%), chemistry, geosciences, biology and applied sciences (constituting the rest 35%). 208 received proposals were admitted for realization.

Scientific results.

1.1. Structure investigations of novel oxide, intermetallic and nanostructured materials

Iron oxides play an important role in the formation of magnetic and other physical properties of the Earth, and find a wide range of technological applications. Recently, a new iron oxide, Fe₄O₅, which can presumably exist in the layers of the Earth's upper mantle, has been synthesized under the combined effect of high pressures and temperatures. A comprehensive study of its physical properties, as well as atomic and magnetic structure using neutron diffraction techniques at the IBR-2 reactor, has revealed a new type of the charge-ordering state with the formation of dimeric and trimeric electronic states in this compound. The phase transition into this state is accompanied by a sharp increase in the electrical resistance and a subsequent change in the symmetry of the magnetic order, namely from a collinear antiferromagnetic (AFM) order to a canting AFM order with a ferromagnetic (FM) component, as well as by a change in the nature of the modulation of the atomic structure, **Fig. 1.1** [1].

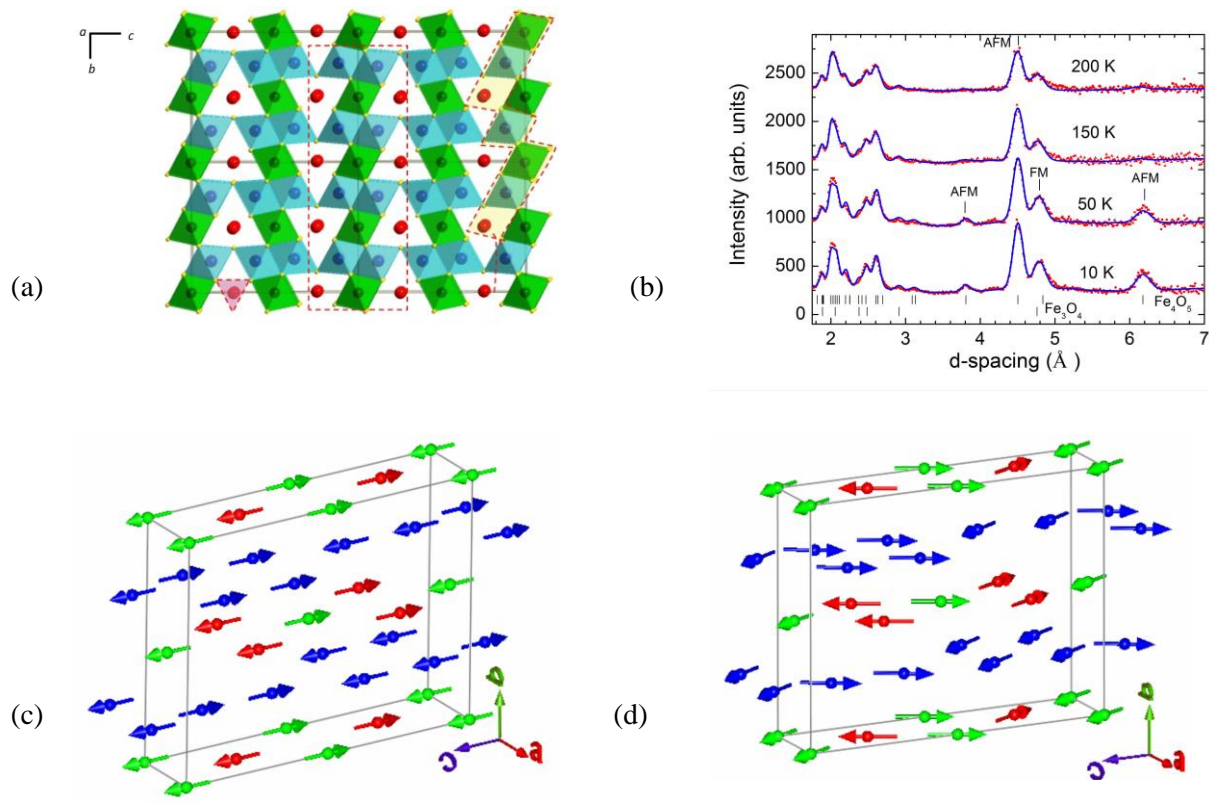


Fig. 1.1. Crystal structure of Fe_4O_5 (a), neutron diffraction spectra obtained at different temperatures and treated by the Rietveld method (b), the magnetic structure at $T = 150$ K (c) and $T = 10$ K (d).

The search for new multiferroics and magnetoelectrics is of current interest in modern condensed matter physics and materials science. A promising system is $\text{BaMn}_{1-x}\text{Ti}_x\text{O}_3$ whose end members are a classical ferroelectric BaTiO_3 with a high Curie temperature ($T_C = 395$ K) and BaMnO_3 – a compound exhibiting a giant magnetoelectric effect and having a relatively high temperature of magnetic ordering ($T_N = 230$ K). The studies of $\text{BaMn}_{1-x}\text{Ti}_x\text{O}_3$ over the entire concentration range $0 < x < 1$ have revealed a very rich structural polymorphism. An increase in the titanium concentration was followed by a sequence of phase transitions between different rhombohedral and hexagonal phases differing by the ratio of oxygen octahedra connected through the corners and edges, 15R - 8H - 9R - 10H - 12R, **Fig. 1.2.** [2,3]. It has been found that the formation of a long-range magnetic order is possible only in structures: 9R, 8H, 15R and at concentrations of $\text{Ti}_x < 0.25$, and the Neel temperature has a very sharp concentration dependence and drops from 230 to 100 K in the given x-range.

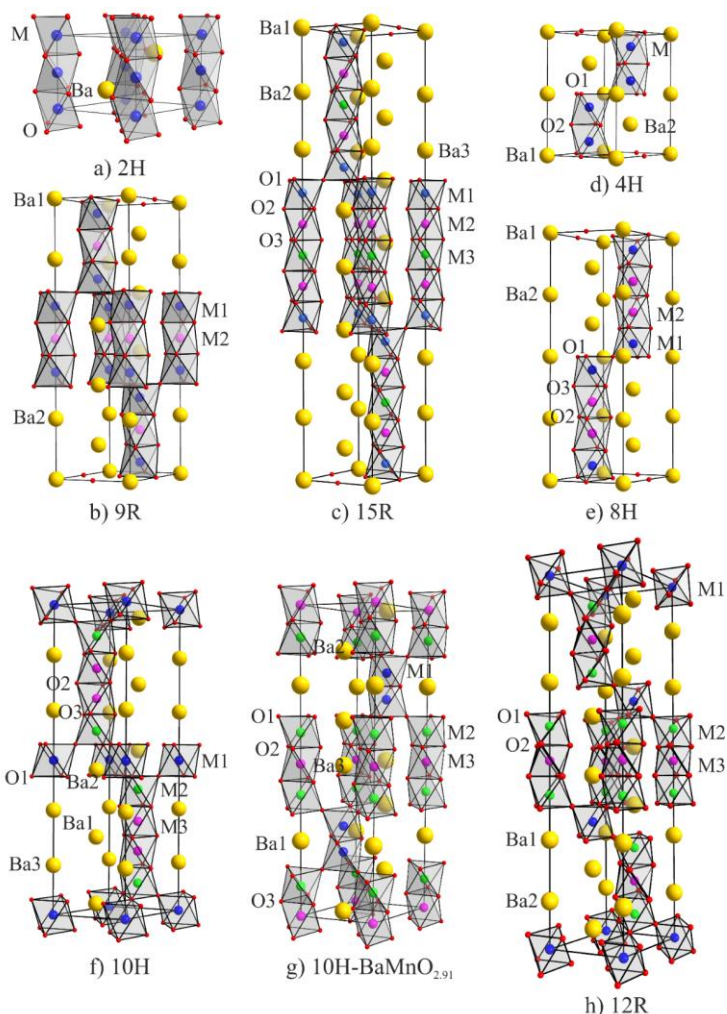
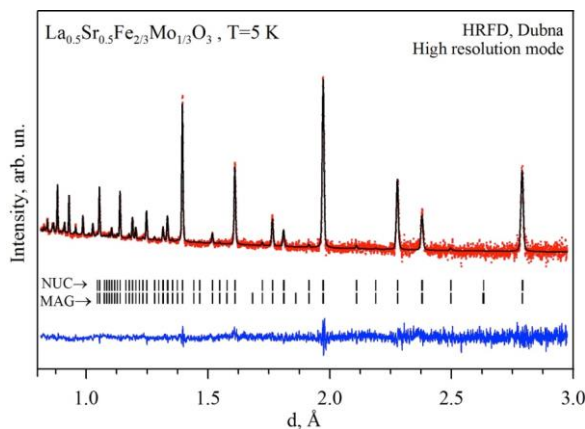
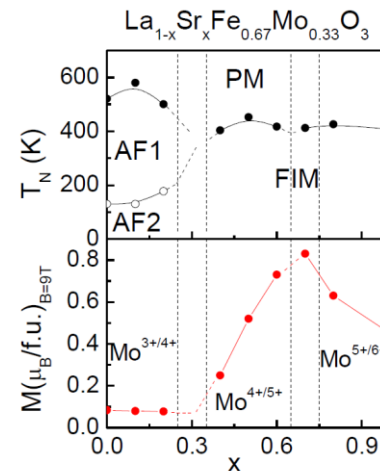


Fig. 1.2. Structure of polymorphic phases in the system $\text{BaMn}_{1-x}\text{Ti}_x\text{O}_3$.

$\text{La}_{1-x}\text{Sr}_x\text{Fe}_{2/3}\text{Mo}_{1/3}\text{O}_3$ ($0 \leq x \leq 1$) perovskites allow exceptionally wide variation of the Mo charge state from +3 ($x = 0$) to +6 ($x = 1$) while the charge state of Fe^{3+} remains virtually unchanged. The end members of this series show antiferromagnetic ordering in $\text{LaFe}_{2/3}\text{Mo}_{1/3}\text{O}_3$ at $T_N = 520$ K and ferrimagnetic ordering in $\text{SrFe}_{2/3}\text{Mo}_{1/3}\text{O}_3$ at $T_C = 420$ K. In both cases, the magnetic structure is dictated by antiferromagnetic superexchange between localized magnetic moments. At intermediate compositions, an interplay of antiferromagnetic-superexchange and double-exchange interactions results in nonmonotonous variations of both the magnetic-ordering temperature and saturation magnetization. To determine the magnetic phase diagram (**Fig. 1.3**) and the cation charge states, neutron diffraction spectra were measured, and XANES data and data on magnetic susceptibility and magnetization were obtained. Also, the magnetic moment per formula unit was determined (**Fig. 1.3**). On the basis of all experimental data, a detailed analysis of the emerging interactions was carried out [4].



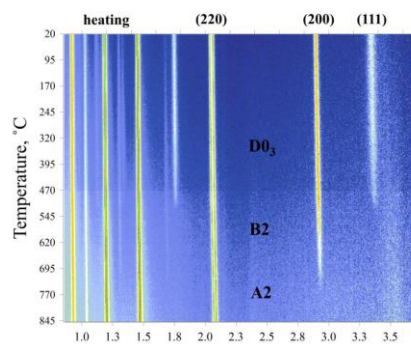
(a)



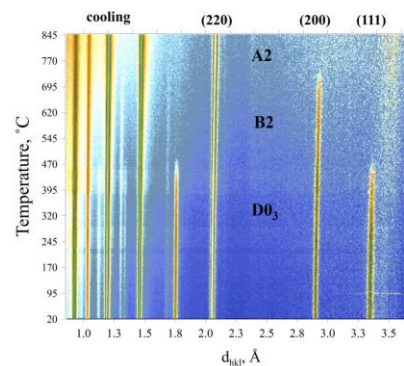
(b)

Fig. 1.3. Neutron diffraction spectrum from $\text{La}_{0.5}\text{Sr}_{0.5}\text{Fe}_{2/3}\text{Mo}_{1/3}\text{O}_3$ treated by the Rietveld method (a). Experimental points, calculated function and difference curve are shown. Dashes show the calculated positions of the nuclear (top row) and magnetic (bottom row) diffraction peaks. The magnetic phase diagram (top) and the magnetic moment value measured at 2 K in a field of 9 T for the $\text{La}_{1-x}\text{Sr}_x\text{Fe}_{2/3}\text{Mo}_{1/3}\text{O}_3$ series (b). Vertical lines separate the regions with different charge states of molybdenum.

Neutron diffraction studies of the $\text{Fe}_{0.735}\text{Al}_{0.265}$ compound were carried out in a wide temperature range (20-900°C) to determine its structural states and atomic ordering mechanism [5], **Fig. 1.4.**



(a)



(b)

Fig. 1.4. 2D representation of structural transitions in Fe-27Al under heating (a) and cooling (b). The initial (before heating) and final (after cooling) conditions – D0_3 phase characterized by the presence of peaks (111) and (200). In the B2 phase the peak (111) is absent, while the peak (200) remains. In the A2 phase both of these peaks are absent. The rates of heating and cooling were ± 2 °C/min, the measurement time of one spectrum – 1 min, i.e. each picture contains about 400 spectra.

The combination of high-resolution diffraction and real-time diffraction made it possible to establish that, in contrast to traditional approaches, the structure of this compound at room temperature is a phase with only partially ordered arrangement (B2) of Fe and Al in a unit cell. A completely ordered phase (Fe_3Al - D0_3 type) is present as clusters of mesoscopic size (~ 200 Å)

coherently incorporated into the matrix of the main phase. After the transition to a disordered state ($T > 740^\circ\text{C}$) and slow cooling to room temperature, the dimensions of the structurally ordered clusters increased to $\sim 900 \text{ \AA}$. A high contrast between the coherent neutron scattering lengths of iron and aluminum made it possible to determine with a good accuracy the temperature dependence of the occupancy factors of sites by Fe and Al atoms up to a phase transition to the disordered state. The obtained results call for further analysis of the equilibrium phase diagram for the Fe-Al system.

1.2. Investigations of magnetic fluids and nanoparticles

A number of experiments on small-angle neutron scattering (SANS) and neutron reflectometry with a horizontal sample plane for the interface of magnetic fluids with silicon (GRAINS) have been carried out in the framework of investigations of the structure and stability of magnetic nanoparticles in bulk and at interfaces, **Fig. 1.5** [6]. It has been found that in the bulk of aqueous ferrofluids stabilized by sodium oleate there are comparatively small (size $\sim 30 \text{ nm}$) and compact aggregates of magnetic particles. When magnetic fluids are modified by biocompatible polymer polyethylene glycol (PEG), cluster reorganization in the bulk of magnetic fluids is observed, namely large and branched clusters (size $> 130 \text{ nm}$, fractal dimension of 2.7) appear. The observed in-bulk reorganization of the magnetic fluids is correlated with the neutron reflectometry data, which is indicative of the formation of a single adsorption layer of magnetic particles on the surface of oxidized silicon in the initial magnetic fluid and the absence of any layer at the ferrofluid/silicon interface after the polymer modification. The study has been performed in collaboration with the Institute of Experimental Physics, Slovak Academy of Sciences (Kosice, Slovakia); the Faculty of Physics of the Taras Shevchenko Kyiv National University (Kiev, Ukraine); the National Institute of Physics and Nuclear Engineering (Bucharest, Romania); Timisoara Branch of the Romanian Academy of Sciences (Timisoara, Romania) and the Max-Planck Institute for Solid State Physics (Stuttgart, Germany).

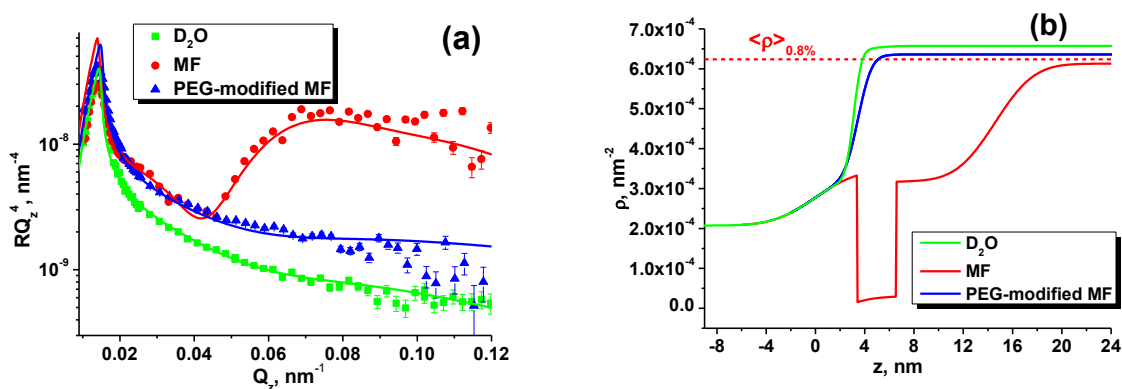


Fig. 1.5. (a) Experimental reflectivity curves for heavy water and magnetic fluids; (b) resulting scattering length density profiles.

In order to improve the synthesis procedure for biocompatible magnetic fluids, SANS (YuMO) and SAXS experiments have been carried out for magnetic fluids prepared using three different methods (**Fig. 1.6**). An important feature of the ferrofluids under study was the addition of a specific component (polysaccharide agarose) to the water-based carrier, which complemented the stabilization effect and also provided biocompatibility of the initial fluids. It has been demonstrated that all investigated magnetic fluids have a complicated and highly aggregated structure, but nevertheless are stable in time. The structures of the magnetic fluids obtained by two methods of synthesis are similar to each other and different from that synthesized using the third method. In the last case two power-law type scattering levels corresponding to mass and surface fractals were observed along with an increase in the characteristic size of magnetic particles.

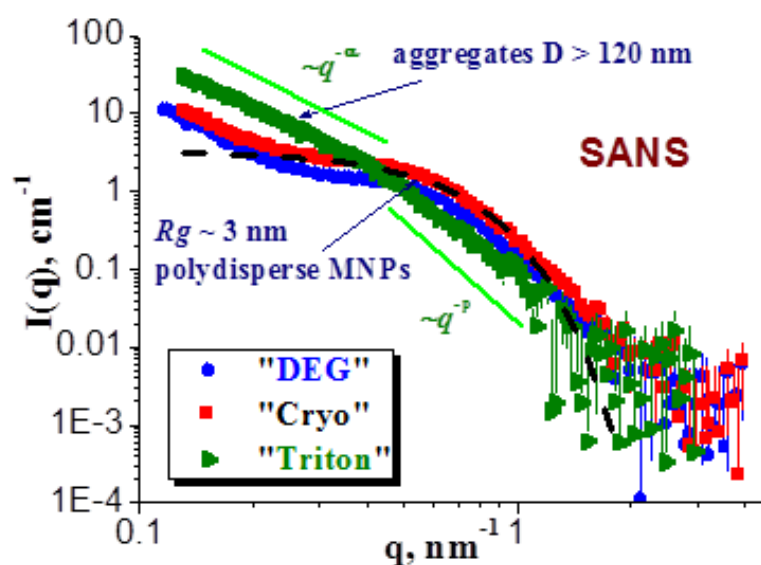


Fig. 1.6. SANS curves for magnetic fluids with agarose synthesized by three different methods. The concentration of magnetite is $\sim 8.8\%$; agarose – 0.1 vol. \% .

The study [7] has been performed in collaboration with the V.I.Vernadsky Institute of General and Inorganic Chemistry (Kiev, Ukraine) and the Department of Physics of the Taras Shevchenko Kyiv National University (Kiev, Ukraine).

1.3. Investigation of layered nanostructures

The biophysical research of fullerene solutions, in particular aqueous solutions of C60 and C70, has been continued. They included the analysis of the cluster structure when placing fullerenes in physiological environment and the study of the interaction of C60 fullerene with antitumor antibiotics, **Fig. 1.7** [8, 9]. Using SANS and tests on mutagenic activity of Doxorubicin and C60 admixture with Doxorubicin on Salmonella Typhimurium TA98 cells it has been shown that fullerene C60 can act as an interceptor of the antitumor antibiotic Doxorubicin and form hetero-complexes with this drug. The research on the interaction of C60 with Doxorubicin,

including SANS, scanning electron (SEM) and atomic force (AFM) microscopy, calorimetry, dynamic light scattering (DLS) and UV-Vis spectroscopy, has been extended to include other aromatic drugs with a similar to Doxorubicin spatial structure such as Landomycin and Cisplatin.

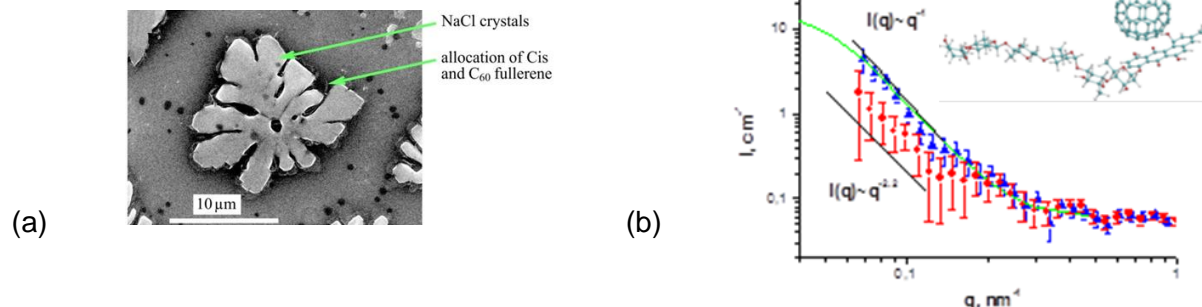


Fig. 1.7. SEM data for C60/Cisplatin solution (a). SANS for aqueous C60 solution (blue triangles) and mixture of C60 with Landomycin A (red circles). The green line corresponds to the model curve obtained from the inverse Fourier transform. Insert: estimated structure of C60 + Landomycin A complex (b).

New effects of the biological interaction of fullerene C60 in combination with various anticancer drugs have been discovered and described. The work was carried out in collaboration with the Departments of Biology and Physics, Taras Shevchenko National University of Kyiv (Kiev, Ukraine).

1.4. Investigation of layered nanostructures

In the framework of the studies on improving the performance of lithium batteries, a series of experiments on neutron reflectometry (GRAINS reflectometer) to study electrochemical interfaces of liquid electrolyte/solid electrode have been carried out (**Fig. 1.8**).

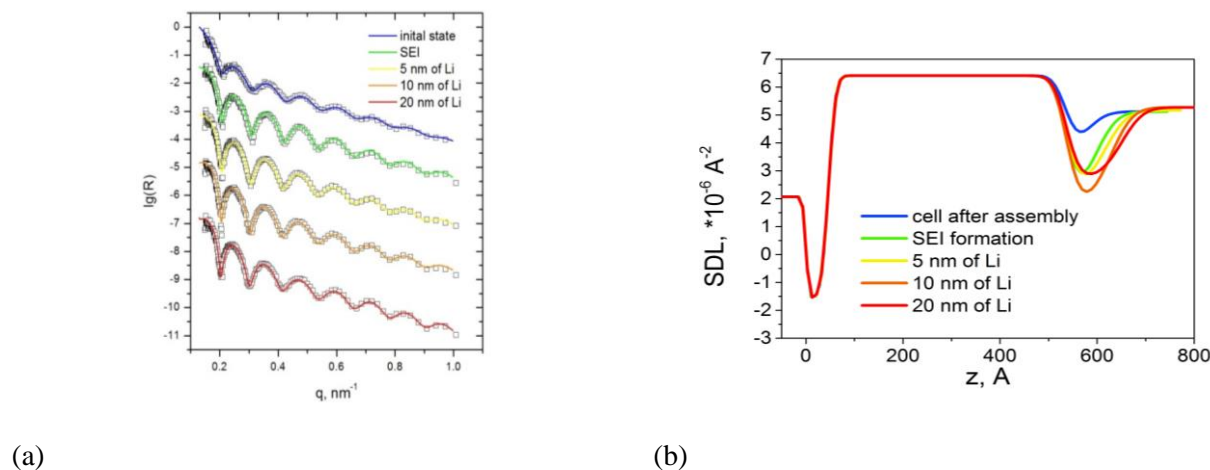


Fig. 1.8. (a) Experimental neutron specular reflectivity curves (points) for a copper electrode at the interface with the electrolyte at different current and voltage supply modes. (b) Resulting scattering length density profiles for different modes presented in (a) with indicated characteristic thicknesses of deposited lithium.

From the specular reflectivity analysis, the formation of a solid-electrolyte interphase (SEI) on the surface of the electrode (Cu) has been concluded, as well as the lithium electrodeposition and growth of parasitic dendritic structures during the operation of an electrochemical cell have been tracked. The obtained profiles of the scattering length density perpendicular to the electrode surface have made it possible to analyze different modes of SEI formation, as well as the formation and growth of nanometer lithium layers of different roughness on the initially formed SEI. It has been shown that neutron reflectometry can be effectively used for *in situ* characterization of lithium plating on metal electrodes [10]. The study has been performed in collaboration with the Department of Chemistry, Moscow State University (Moscow, Russia).

In layered structures S1/FM/S2 consisting of ferromagnetic and superconducting layers, the effect of superconductivity on ferromagnetism has been studied by using reflectivity and scattering of polarized neutrons. It has been shown experimentally that at low temperatures magnetic structures with linear dimensions in the range from 5 nm to 30 μm are formed. At temperatures below the superconducting transition, the magnetization of the magnetic structures in the vanadium and niobium layers is suppressed by superconductivity. **Figure 1.9** demonstrates for different structures that the neutron scattering diminishes as the temperature decreases from 8 to 1.5 K.

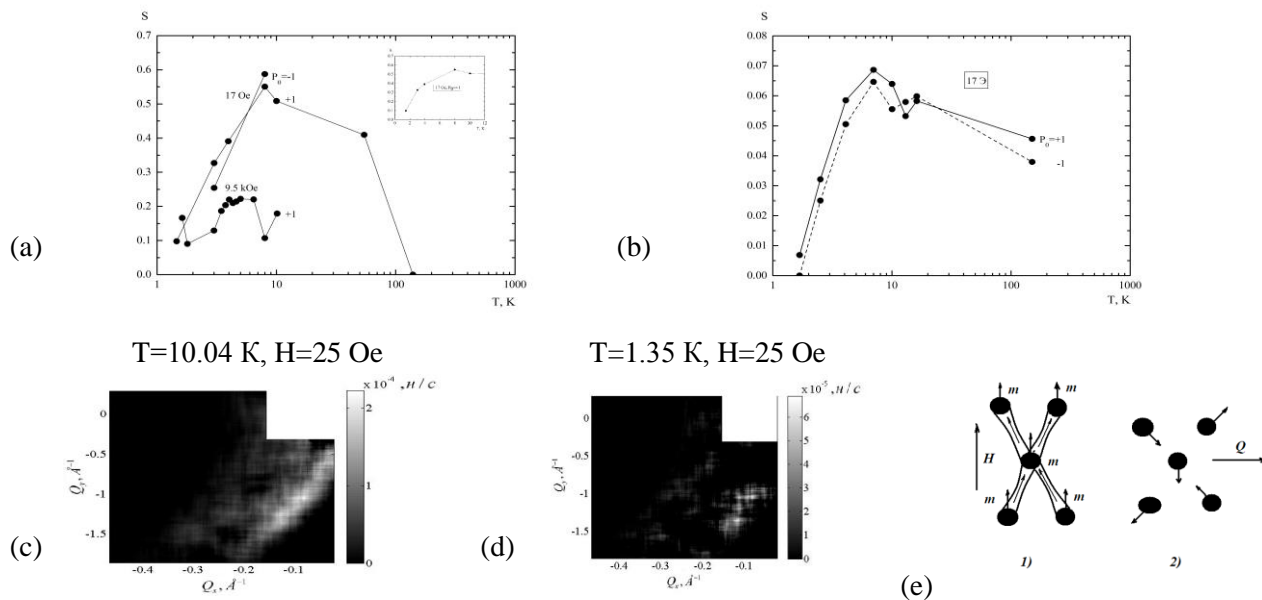


Fig. 1.9. Dependence of the neutron scattering coefficient $S(T)$ for the structure V(150nm)/(FM(7%)+V(50%)+Nb(43%))(25 nm)/Nb(150 nm) at $H = 17$ Oe and 9.5 kOe (a). The dependence of the neutron scattering coefficient $S(T)$ for the structure V(150nm)/(FM(7%)+V(43%)+Nb(43%)+Cr(7%))(25 nm)/Nb(150 nm) at $H = 17$ Oe (b). The contours of the neutron scattering intensity on the plane of transfer wave vectors Q_y - Q_x at $H = 25$ Oe and $T = 10.04$ K (c) and 1.35 K (d). The structure of the cluster system at 8 K (1) and 1.5 K (2) (e).

Also, **Fig. 1.9** shows how the structure of the cluster system at 8K is transformed into the structure at 1.5 K.

Using the *in situ* reflectometry of polarized neutrons the magnetic state of a superconducting-ferromagnetic layered structure Ta/V/FM/Nb/Si has been studied. The relaxation of a non-uniform magnetic state of the structure with a characteristic time of a few hours was observed at temperatures both above and below the superconducting transition points in the structure layers. The character of the time dependence of the neutron scattering depends on the magnitude of the magnetic field H , temperature and neutron polarization. **Figure 1.10** shows the time dependence for the coefficient of neutron scattering. The dependence on polarization due to the scattering from magnetic clusters can be seen. The moments of the clusters are reoriented from the initial direction along the field to the direction the field. There is also a scattering contribution which is independent of polarization and caused by the formation of a domain structure with time.

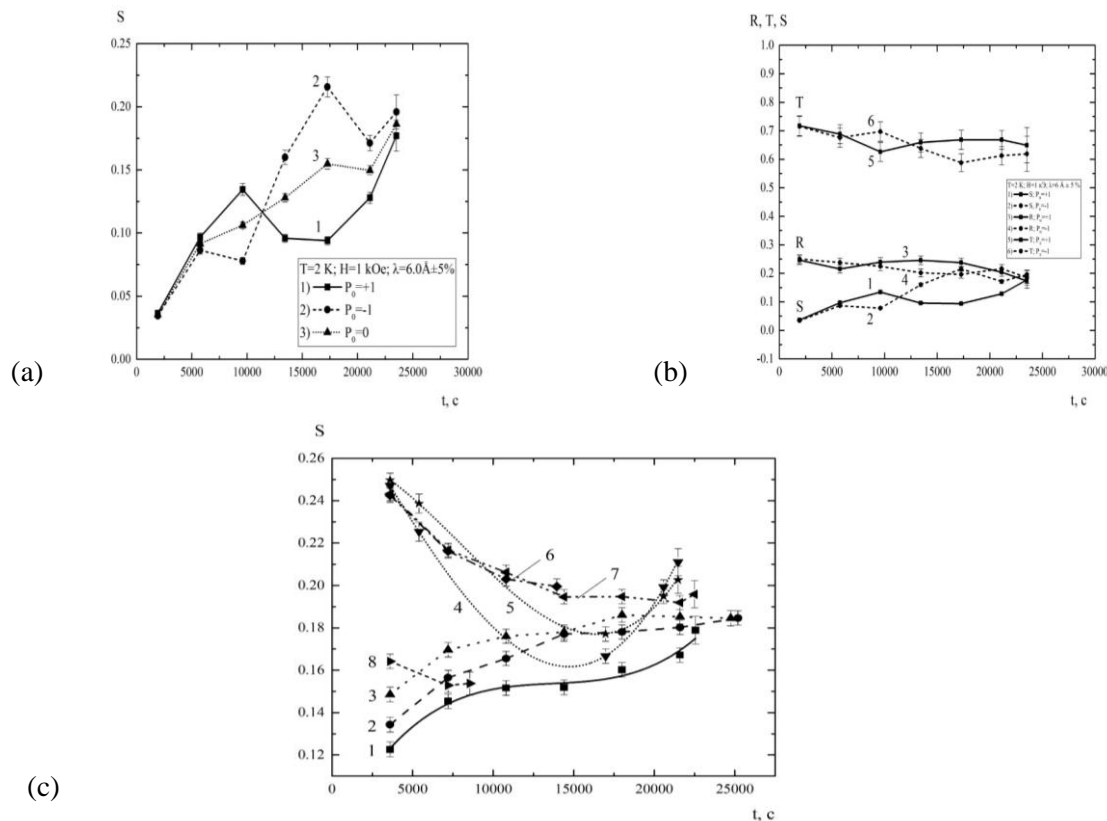


Fig. 1.10. Dependence $S(t)$ in magnetic field of 1 kOe at temperature of 2 K for $\lambda = 6 \text{ \AA}$ and $P_0 = +1, -1$ and 0 (a). Time dependences for coefficients of transmission T , reflection R and scattering S (b). Dependence $S(t)$ at $T = 3 \text{ K}$: $P_0 = +1$ at H -values: 17 Oe (1), 1 kOe (2), 2 kOe (3), 4 kOe (4), 6 kOe (6), 7 kOe (7) and 8 kOe (8); $P_0 = -1$ and $H = 4 \text{ kOe}$ (5) (c).

At a large field of 4 kOe (curves 4 and 5, **Fig. 1.10c**), in early stages there is a depinning of superconducting vortices in the mixed state of superconducting layers of vanadium and niobium, which is changed to the motion of cluster moments. Thus, apparently it was for the first time when neutron reflectometry (coherent propagation - reflection and transmission, as well as GISANS) was used to study the relaxation of the magnetic state and observe relaxation in a hybrid structure consisting of ferromagnetic and superconducting layers. In this case, the



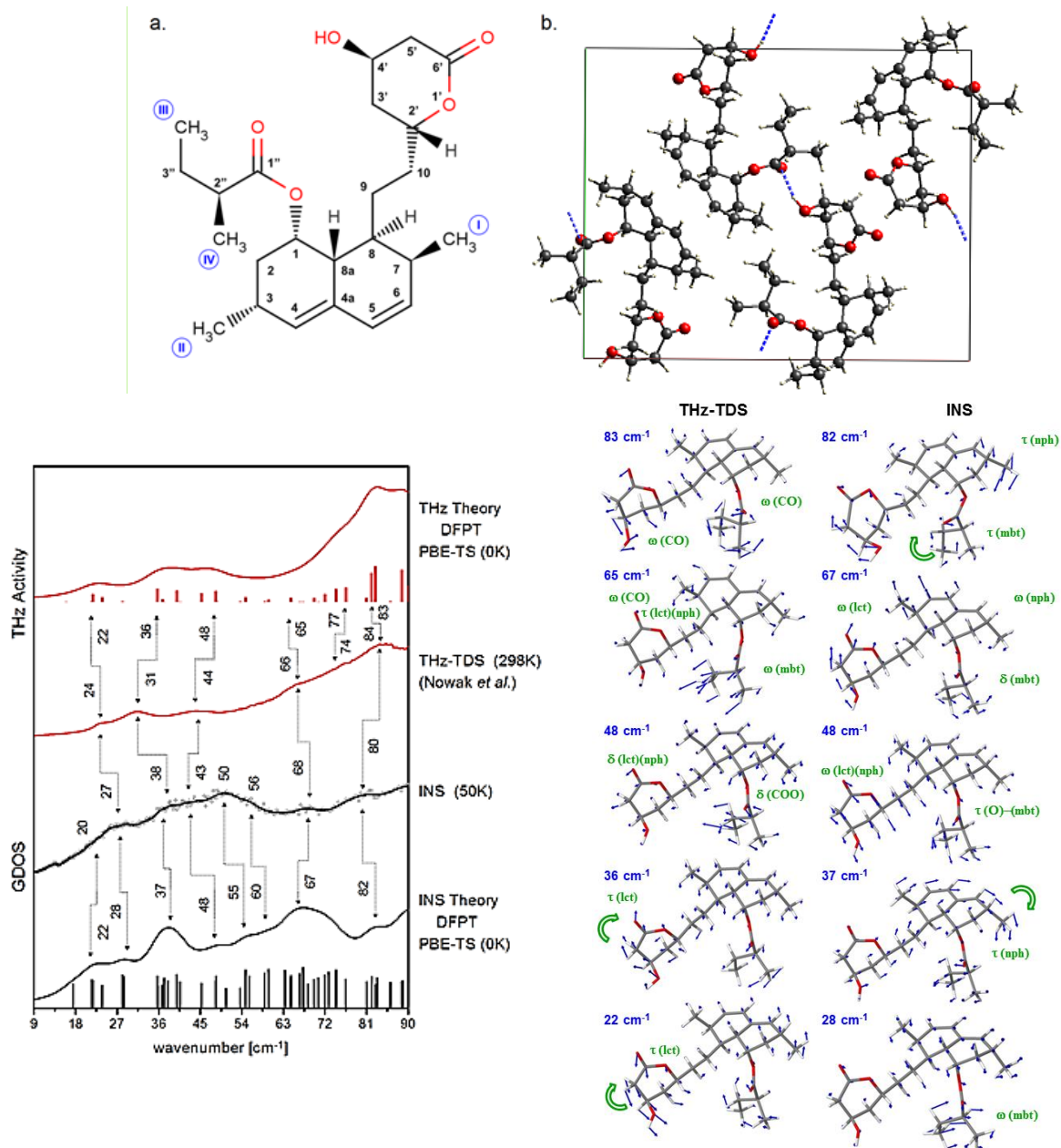
characteristic time of the change in the magnetic state of the systems of clusters, domains and vortices was a few hours with a several percent accuracy in the time dependence measurement. The measurement of the time dependences for the coefficients of scattering, reflection and transmission occurring under changes in the average and local potentials of the interaction of neutrons with the medium, was an effective method for identifying types of magnetic systems in the layered structures. In principle, a potential increase in the intensity of the neutron beam at the REMUR spectrometer used in the present study could allow one to achieve time resolution of a few minutes in studies of irreversible processes.

1.5. Investigation of biological nanosystems, lipid membranes and lipid complexes

It is well known that fermentative systems of oxidative phosphorylation in mitochondria can operate in two states - in a state of supercomplex and in a dissociated state. The comprehensive studies have shown that heart mitochondria operate in the state of supercomplex in a wide range of tonicities of incubation media. This result has been obtained by the polarographic method using the double inhibitor technique by Baum. The investigation of mitochondrial ultrastructure by the methods of electron microscopy (EM) and small-angle neutron scattering (SANS) under conditions of normal tonicity (300 mOsm - isotonia) and low-amplitude swelling (120 mOsm - hypotonia) has proved the existence of two types of mitochondrial ultrastructure. Using EM, it has been found that the mitochondrial cristae in hypotonic and isotonic conditions have different shape and thickness. The tomography method has demonstrated a folded configuration of the cristae. The studies of the ultrastructure of heart mitochondria by methods of EM and inhibition analysis have been carried out on intact functioning mitochondria in the presence of respiratory substrates. Using the SANS method it has been shown that in hypotonic and isotonic media highly-organized lipid-protein lamellar structures are formed in mitochondria. The formation of lipid structures has been demonstrated by using the contrast variation technique (variation of the fraction of heavy water in a solution). Also, it has been shown that the thickness of the mitochondrial cristae depends on the medium tonicity. Thus, the data obtained from the investigation of the functioning and structure of mitochondria suggest the existence of two states for the system of oxidative phosphorylation, which forms cristae with different structural parameters [11].

1.6. Atomic and molecular dynamics

Inhibitors of 3-hydroxy-3-methylglutaryl coenzyme A (HMG-CoA) reductase are among the most effective and widely used drugs for lowering the cholesterol level, known as statins. Statin monotherapy is generally well tolerated and has minimal side effects. The first HMG-CoA inhibitor approved by FDA (Food and Drug Administration, USA) – lovastatin (MEVACOR®; ALTOCOR® & ALTOPREV®), below referred to as LOV was mainly used to control hypercholesterolemia (**Fig. 1.11**).



(c) (d)
Fig. 1.11. Molecular formula of lovastatin (LOV; (1S,3R,7S,8S,8aR)-8-{2-[(2R,4R)-4-Hydroxy-6-oxooxan-2-yl]ethyl}-3,7-dimethyl-1,2,3,7,8,8a-hexahydronaphthalen-1-yl (2S)-2-methylbutanoate) with marked methyl groups (I-IV) (a). Crystal structure of lovastatin (space group $P2_12_12_1$) optimized using PW - DFT (PBE-TS) (b). Comparison of theoretically calculated (harmonic approximation DFPT PBE-TS) and experimental vibrational spectra of lovastatin according to the data of neutron (IINS) and optical terahertz spectroscopy (data by Nowak *et al.* Acta Poloniae Pharmaceutica in Drug Research, Vol. 72 No. 5 (2015) pp. 851-866) (c). The most important vibrational modes of lovastatin contributing to the INS and THz-TDS spectra. The eigenvectors obtained from the harmonic PBE-TS calculations are shown in the projection of one molecule.

In the LOV molecule three main parts can be distinguished – lactone ring (lct), naphthalene fragment (nph) and methylbutanoate chain (mbt). The molecules are linked by hydrogen bonds $O\cdots HO$ (**Fig. 1.11**). Hydrogen bonds bind lactone rings (methyl group) with methylbutanoate chains (carbonyl group). The second carbonyl group of lactone rings is unbound.

In collaboration with the Adam Mickiewicz University (Poznan, Poland), atomic and molecular dynamics of lovastatin has been studied by 1H NMR and inelastic neutron scattering complemented by theoretical ab-initio calculations using the PW-DFT method. A consistent molecular dynamics model has been obtained, which can be later used to describe the dynamics of other alternative drug forms and tendencies to amorphization. It has been found that the molecular dynamics of lovastatin is determined by the motions of methyl groups and the conformational disorder in the methylbutanoate fragment. The vibrational dynamics of lovastatin was analyzed focusing on the energy transfer range with low wave numbers, which was experimentally studied by neutron (INS) and terahertz (THz-TDS) spectroscopy. The theoretical calculations made it possible for the first time to describe with a high accuracy the phonon spectrum of lovastatin in this region (**Fig. 1.11**). It should be noted that the main contribution to the inelastic neutron scattering spectra is from vibrations of hydrogen-containing molecular groups, which are the most mobile ones for the movable mbt fragment contributing to the most intense vibrational mode. At the same time, the primary contribution to the terahertz spectra is from the most polar molecular groups containing oxygen and included in the lct fragment. The corresponding normal vibrational modes are shown in **Fig. 1.11**. The most intensive spectral features for THz-TDS are due to the modes related to the vibrations of hydrogen bridges $O\cdots O$ in a range of above 65 cm^{-1} , while the modes in a range of below 65 cm^{-1} are determined by the vibrations of the whole lct fragment. This set of modes is of a general nature without intending to be bound to a particular LOV compound and can be used in further studies of statins.

1.7. Applied research

On FSD, the experiments to study the distribution of residual stresses in welds after using various welding methods have been continued. The work has been carried out in collaboration with the Institute of Electronics, BAS (Sofia, Bulgaria) and the Brandenburg University of Technology (Germany). In 2016, residual stresses were measured in a massive (thickness ~ 20 mm) sample from structural steel S355J2+N welded with combined multipass welding: 1st pass – metal welding in shielding gases (MSG-welding), 2nd and 3rd passes – submerged arc welding (SAW-welding), **Fig. 1.12**.

In neutron experiments with new radial collimators in the middle part of the sample the residual stress tensor components were measured in a wide X-range across the weld, which were further used to determine the residual stress values (**Fig. 1.12**). The maximum component is the longitudinal stress tensor component σ_x (~ 550 MPa) directed along the weld which is of the stretching character in the center of the weld. The level of the transverse component of the stress tensor σ_y is significantly lower (~ 350 MPa), and the level of the normal component σ_z does not exceed 180 MPa.

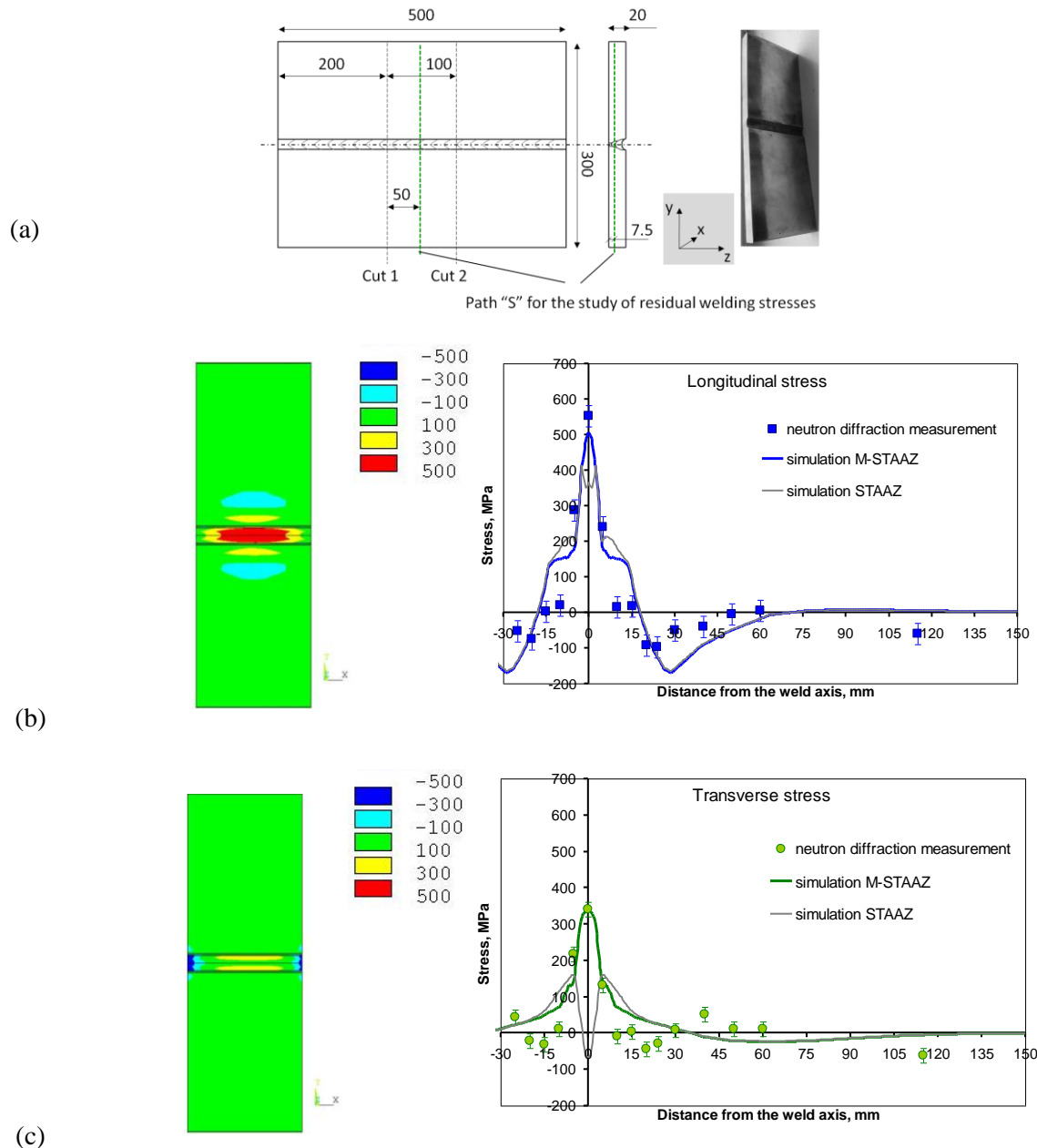


Fig. 1.12. Sample cut from a thick (~ 20 mm) plate welded with multi-pass submerged arc welding (SAW-welding). "S" is a scan-line in neutron measurements. Arrows indicate the strain tensor components (X, Y, Z) (a). Full map of distribution of the longitudinal component (σ_x) in the tensor of residual stresses calculated by the finite element method (FEM) and the comparison of the experimentally measured σ_x -values along the scan-line "S" with the results of numerical modeling by the finite element method FEM (solid line) (b). Full map of distribution of the transverse component (σ_y) in the tensor of residual stresses calculated by the finite element method (FEM) and the comparison of the experimentally measured σ_y -values along the scan-line "S" with the results of the numerical modeling by the finite element method FEM (solid line) (c).

In addition to the experiments on neutron diffraction, numerical calculations by the STAAZ method have been performed in the framework of the existing cooperation with the research group of Prof. V. Mikhailov (Brandenburg University of Technology, Germany). The comparison of the neutron data and FEM calculations has shown good agreement, indicating the reliability of the developed theoretical model for the multi-pass welding process. This information can serve as a basis for the development of specific technical recommendations to achieve the desired level and profile of residual stresses.

On FSD, a series of TRIP-composites with austenitic matrix and different content of reinforcing ceramic phase of zirconium dioxide ZrO_2 partially stabilized by magnesium (Mg-PSZ) have been investigated at various degrees of plastic deformation (uniaxial compressive load), **Fig. 1.13**. The study has been done in collaboration with the Freiberg University of Mining and Technology (Freiberg, Germany). At the load values above 650 MPa, the formation of two phases in the austenitic matrix was observed: cubic α' -martensite and hexagonal ϵ -martensite. The content of ϵ -martensite reached $\sim 15\%$ for all samples under deformation up to $\sigma = 1100$ MPa and then remained almost unchanged until the maximum load values of $\sigma = 1580$ MPa. In contrast, the α' -martensite phase exhibited a monotonic increase in the load range from 950 to 1580 MPa. In the ceramic sample of pure zirconium dioxide (100% ZrO_2) two phases were observed: cubic ($f \approx 55\%$) and tetragonal ($f \approx 45\%$). The residual deformation of the crystal lattice of the austenitic matrix is of compressive character and increases up to $\sim 10^{-3}$. In this case, the crystal lattice deformation in α' - and ϵ -martensites is more complex and reflects the redistribution of the load between the phases. Furthermore, under the deformation in the range from 650 to 1580 MPa a noticeable broadening of the diffraction peaks with increasing plastic deformation was observed, which was caused by the variation in the contrast factor of dislocations. For the austenitic matrix the dislocation densities were evaluated from the peak broadening. They reached the values in the range of $12\text{--}20 \cdot 10^{14} \text{ m}^{-2}$ depending on the content of zirconium dioxide in the composite.

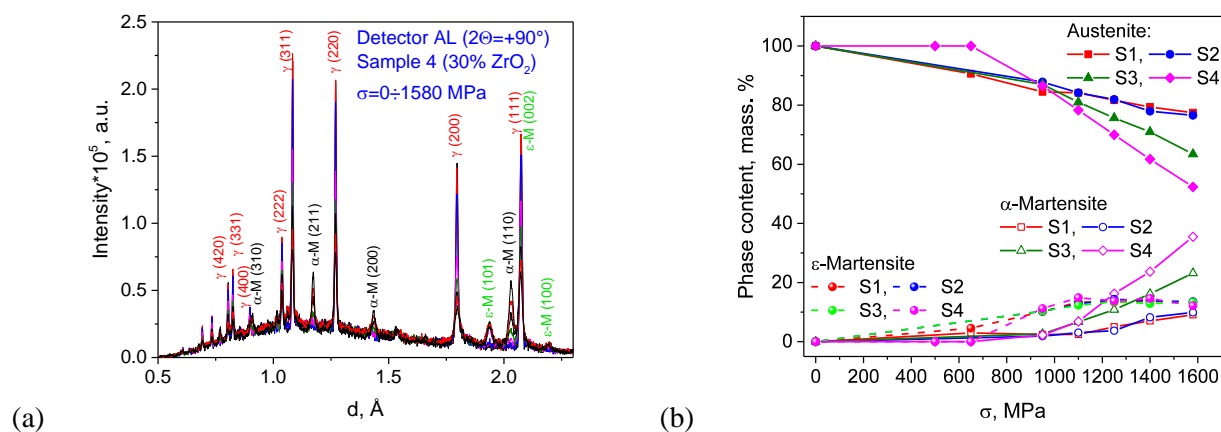


Fig. 1.13. The change in the diffraction spectra of the TRIP-composites as a function of plastic deformation (a). The change in the phase mass content in the TRIP composites depending on the degree of plastic deformation (b).

The texture and microstructure of the pristine and retrogressed samples of eclogite and surrounding metasediments have been investigated to gain insights into the deformation processes in the palaeo-subduction channel of the Tauern region (Austria), **Fig. 1.14** [12]. The texture features and deformation processes in omphacite and glaucophane have been analyzed. The presence of a plastic deformation cycle in the metamorphism of eclogite and blueschist facies associated with the subduction and exhumation of rocks has been established.

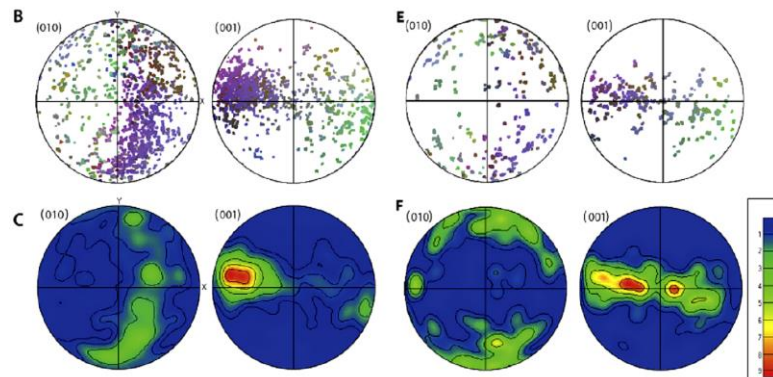


Fig. 1.14. Pole figures for eclogite rocks obtained with the SKAT diffractometer.

The work has been done on the development of the methodology for evaluating the amount of residual austenite in high strength steels using the neutron diffraction method. The neutron diffraction spectra were measured on the texture instrument SKAT at FLNP JINR in order to eliminate the influence of the texture on the results. The measurements of calibration samples with the known austenite content were made. Using the results from the measurements of these samples, the calibration lines were obtained and applied to determine the fraction of residual austenite in the samples of medium-carbon steels (0.3 to 0.4%) with a tensile strength of 1500 MPa and 1700 MPa at different annealing temperatures (150 to 400°C) following the hardening treatment [13].

On the EPSILON diffractometer, *in-situ* experiments to study the dependence of deformation on the load on a cylindrical sample of sandstone have been carried out (**Fig. 1.15**).

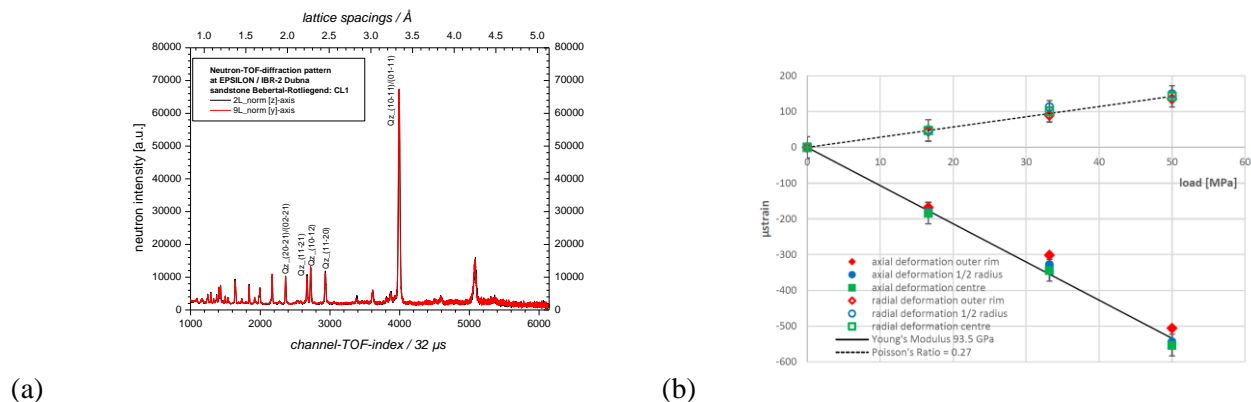


Fig. 1.15. Neutron diffraction spectra of sandstone measured on the EPSILON diffractometer (a). Dependence of microstresses on the load at various deformation types (b).

A load of up to 56.33 MPa was applied during 9 stages to determine the Young's modulus for the crystallographic planes of quartz (01-11), (10-11), (11-20), (01-12)/(10-12). These results are consistent with the Hooke's law [14]. Instead of traditional fitting of diffraction data using the Rietveld method, an elastomechanical model has been developed to describe the stress-strain behavior, taking into account the changes in the pore space as a result of compaction of sediments associated with the change in the shape of quartz grains. This model was used to calculate the displacement of the diffraction peaks in the Voigt or Reuss approximations and their combinations. It has been established that the developed model can simulate with a high accuracy the diffraction data under load using the data measured without load including both the displacement of peaks and their half-width changes [15].

2. MULTIMODAL PLATFORM FOR RAMAN AND NONLINEAR OPTICAL MICROSCOPY AND MICROSPECTROSCOPY FOR CONDENSED MATTER STUDIES

In 2016, the research activities of the Raman Spectroscopy Sector were focused mainly on accomplishing the following objectives:

- highly sensitive, contrast, and, most notably, noninvasive imaging of biological samples using Raman scattering microscopy and nonlinear optics methods (CARS, SHG);
- further increase in the concentration sensitivity limit of sample measurements by the SERS method at a level no worse than 10^{-10} M;
- acquisition of new data on photo- and upconversion luminescence in glass-ceramics based on nanosized ZnO crystals doped with rare-earth elements.

2.1. In the reporting period, the work (started in 2015) on highly sensitive and high-speed visualization of protein crystals using the polarized coherent anti-Stokes Raman scattering (P-CARS) and the second harmonic generation (SHG) was completed. Thus, CARS, especially P-CARS, can be successfully applied for fast, high-resolution, high-contrast and very informative imaging of protein crystals. The CARS and SHG images are composed of 500×500 pixels taken by raster scanning the sample. Signal integration time was 3 μ s/pixel.

2.2. During the period under review considerable advances have been made in SERS research. In particular, the concentration sensitivity limit at a level of 10^{-10} M has been obtained for DNA molecules. It is 2–3 orders of magnitude better than in 2015. The results of these studies suggest that the classical spectra of DNA molecules can be found by the SERS substrate mapping. Moreover, the prospects for the DNA detection by the SERS spectroscopy with lasers of 473, 633, and 785 nm wavelengths are very encouraging. To our knowledge, the detection of such a small amount of DNA has not been reported previously.

2.3. In transparent glass-ceramics from the potassium-zinc-aluminum-silicate system co-doped with rare-earth ions (europium, ytterbium) and containing ZnO nanocrystals, strong red (~612 nm) luminescence in the visible region from intracenter transitions on Eu^{3+} ions and ultraviolet exciton luminescence (~380 nm) from ZnO crystals have been simultaneously

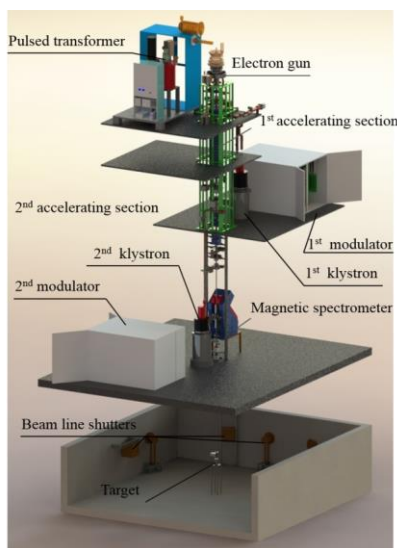
observed for the first time. Luminescence from triply charged europium ions has never been studied for this type of glass-ceramics.

3. NEUTRON NUCLEAR PHYSICS

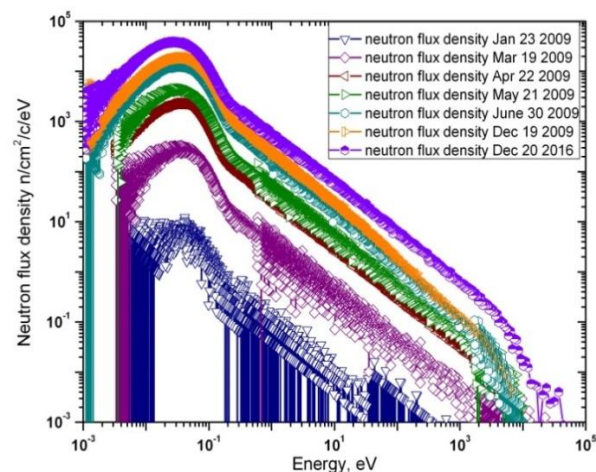
In 2016, in FLNP the scientific activity in the field of neutron nuclear physics was carried out in the following traditional directions: investigations of time and space parity violation processes in neutron-nuclear interactions; studies of the fission process; experimental and theoretical investigations of fundamental properties of the neutron; gamma-spectroscopy of neutron-nuclear interactions; atomic nuclear structure, obtaining of new data for reactor applications and nuclear astrophysics; experiments with ultracold neutrons, applied research using NAA. The scientific program to study the inelastic scattering of fast neutrons made into a separate project "TANGRA" was successfully implemented. A number of investigations in the field of fundamental physics and ultracold neutron physics were performed on the neutron beams of nuclear research centers in Germany, China, USA, France, Switzerland.

3.1. Modernization of the IREN facility.

At the end of 2015 the second accelerating section was installed instead of the drift gap at the LUE-200 accelerator. In the early 2016 the connection of technical systems for the second accelerating section was made and a complex check of all systems of the accelerator was done. The existing accelerator configuration: the first section is powered by an E3730A Toshiba klystron, the second one – by a 2129 Thomson klystron. The power supply of klystrons is provided by Dawonsys modulators (**Fig.3.1.**).



(a)



(b)

Fig. 3.1. (a) Scheme of new accelerator configuration. (b) Spectra of neutron flux density from the IREN obtained during development of the facility

During 2016 the training of the accelerating systems with the gradual achievement of nominal operating parameters was carried out. In December the facility operated within nominal parameters at a frequency of 50 Hz without any failures during one week. Preliminary measurements of the neutron flux were carried out. The estimation showed an increase of the neutron yield by at least 3 times in comparison with the operation with one section.

Experimental and methodological investigations.

3.1. Investigation of the mechanism of fragment excitation and prompt neutron emission and gamma-ray cascades by simultaneous spectroscopy of fission fragments, neutrons and gamma-rays.

A setup has been designed to study the prompt neutron emission and gamma-ray cascades for the fragments with defined masses in coincidence with PFN in the resonance neutron induced fission of ^{235}U . It consists of a double ionization chamber with Frisch grids, an NE-213-scintillator-based fast neutron detector, a pair of gamma-ray NaI-based scintillation detectors. The data acquisition system was implemented on the basis of an eight-channel system of synchronized pulse digitizers with a sampling rate of 250 MHz and amplitude resolution of 12 bits. The calibration experiments were carried out in the period from December 2015 to March 2016 on the IBR-2 thermal neutron beamline. At present, the data analysis and the setup upgrade involving the replacement of two NaI detectors with high-purity germanium detectors are in progress.

3.2. Investigations of (n,p), (n, α) reactions

The experimental and theoretical investigations of the (neutron, charged particle) reactions induced by fast neutrons have been conducted. The experiments were carried out at the Van de Graaf accelerators EG-5 in FLNP JINR and EG-4.5 of the Institute of Heavy Ion Physics of Peking University. Data on the reactions with the emission of charged particles induced by fast neutrons are of much interest for studying the mechanisms of nuclear reactions and atomic nuclear structure as well as in choosing engineering materials and in performing calculations in the development of new facilities for nuclear power engineering.

The analysis of the data from the measurements of the $^{144}\text{Sm}(n,\alpha)^{141}\text{Nd}$ and $^{66}\text{Zn}(n,\alpha)^{63}\text{Ni}$ reactions at $E_n = 4.0, 5.0$ and 6.0 MeV has been completed. The data have been obtained for the first time. The experimental cross-sections have been compared with the available libraries and calculations using the TALYS-1.6 code (**Fig. 3.2**).

A systematic analysis of our experimental cross-sections of the (n, α) reaction in the energy range from 4 to 6.5 MeV has been performed. The results of the analysis can be used in astrophysical calculations, e.g. for the s-process, helium burning, and also allow one to estimate the cross-sections of unstable isotopes for which the measurements are difficult or impossible.

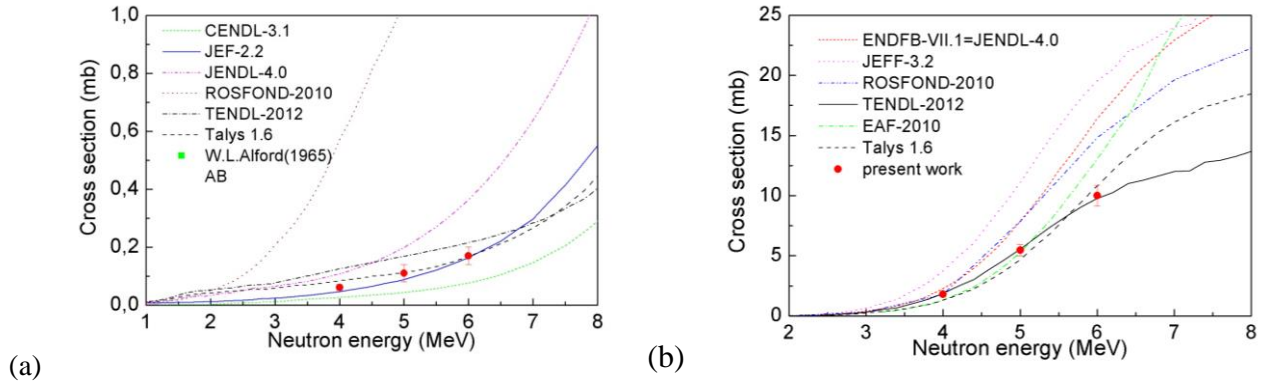


Fig. 3.2. Cross-section of the: (a) $^{144}\text{Sm}(n,\alpha)^{141}\text{Nd}$ reaction in comparison with the existing measurements and estimates for the neutron energy range from 1.0 to 8.0 MeV; (b) $^{66}\text{Zn}(n,\alpha)^{63}\text{Ni}$ reaction in comparison with the existing measurements and estimates for the neutron energy range from 2.0 to 8.0 MeV.

3.3. Measurements of gamma-spectra and angular distributions of gamma-rays for various nuclei using the tagged neutron method

In the framework of the "TANGRA" project, the angular correlations of γ -rays and neutrons, as well as gamma-spectra produced in the inelastic scattering of 14.1 MeV neutrons by various nuclei have been measured. These measurements are aimed at determining the partial cross-sections of the formation of nucleus excitation levels with the corresponding gamma-lines in inelastic neutron scattering reactions, as well as spin characteristics of these levels in the given reaction. This information is important for further development of the method of elemental analysis using tagged neutrons, in particular, to create a local database of characteristic gamma-rays for a broad set of elements, and for a detailed study of inelastic scattering reactions of fast neutrons by these nuclei.

3.4. Measurement of T-odd effects in ^{235}U fission on a hot source of polarized neutrons

In the framework of the FLNP-ITEP-FRM2 collaboration a series of experiments were continued to measure the ROT-effect in the emission of prompt γ -rays and neutrons in the binary fission of ^{235}U and ^{233}U induced by polarized cold neutrons. The experiments with 0.3-eV neutrons were carried out on the POLI instrument at the FRM-2 reactor (Garching, Germany). Fragments were detected by fast multi-wire detectors and could be separated into light and heavy ones by the time of flight. Gamma-rays and neutrons were detected by scintillation counters placed at specific angles to the direction of emission of the fragments. The effect of rotation of the fissioning system in or against the direction of the angular momentum transferred by a polarized neutron for gamma-rays and neutrons was measured. The effect was measured for 9 days. As a result, the effect values (averaged over all detector position angles) were obtained: for gamma-rays — $(-4.6 \pm 2.7) \times 10^{-5}$; for neutrons — $(2.7 \pm 2.9) \times 10^{-5}$. A new experiment is planned, in which we expect to observe the effect or determine its upper limit with the accuracy comparable to that obtained on the cold neutron beam.

3.5. Measurement of the coefficients of P-odd angular correlations in the reactions of cold polarized neutrons with light nuclei

The measurement of P-odd asymmetry in the emission of α -particles in the $^{10}\text{B}(n,\alpha)^7\text{Li}$ reaction was carried out on the cold polarized neutron beam of the PF1B instrument at the ILL reactor (Grenoble, France). A 24-section ionization chamber with insensitive gas gaps was used as a detector of α -particles. The P-odd asymmetry value was found to be $\alpha_{P\text{-odd}}^{^{10}\text{B},\alpha} = -(11.2 \pm 3.4) \cdot 10^{-8}$. The result has been obtained for the first time in the world. This is only the second nucleus after ^6Li for which the P-odd effect was discovered.

3.6. Experiment to obtain a focused beam of very cold neutrons using a reflector of diamond nanoparticles

Ultracold neutrons (UCN) and very cold neutrons (VCN) intensively interact with nanoparticles due to the fact that the neutron wavelength and the particle size are of the same order of magnitude. One of the practical applications of nanoparticle reflectors can be a sharp increase in the VCN yield from the source, if we manage to form a narrow beam from the isotropic distribution and direct it to a neutron guide. In order to determine the possibility of the formation of such beams, a specialized experiment was carried out. A beam of very cold neutrons passes through a velocity selector and comes to the bottom of the trap through the inlet opening. The trap is a thick-walled tube with its walls consisting of nanodiamond powder. Neutrons confined in a trap can be detected by a position-sensitive detector mounted on its exit end. The preliminary results have shown that the number of escaping neutrons is $\sim 1\text{-}2\%$ of the number of neutrons entering the trap, with the yield increasing as the neutron energy decreases. The beam formed has an angular divergence of $10^{-2}\text{-}10^{-3}$ rad. These results indicate that the covering of a VCN source with a nanoparticle reflector can result in an increase in the number of VCN in the neutron guide by many factors of ten.

3.7. Experiment to study quasi-specular reflection of cold neutrons from the surface of nanopowder

For cold neutrons falling on the surface of a nanopowder a quasi-specular reflection can also be observed. We experimentally measured the parameters of this phenomenon using the reflection of neutrons from a nanodiamond powder. For this purpose, we measured the dependence of the angular distribution of reflected neutrons for different wavelengths of incident neutrons and different angles of incidence (1° , 2° , 3° and 4°) of the neutron beam on the surface. The measurements were performed for a powder of nanoparticles of different sizes. From the data presented in **Fig.3.3** it can be seen that for neutrons with longer wavelengths a more efficient reflector is that with large nanoparticles, for neutrons with shorter wavelengths – with small nanoparticles.

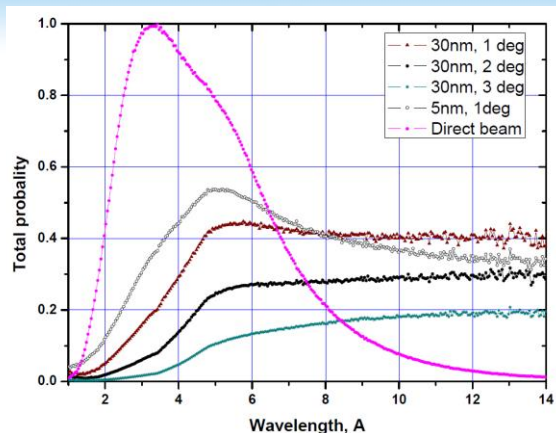


Fig.3.3. Total probability of reflection from the surface of nanopowders as a function of neutron wavelength for angles of incidence of 1°, 2° and 3°. The data for powders of two kinds of nanoparticles with an average size of 30 nm and 5 nm are presented.

The findings can help in the construction of primary sections of mirror neutron guides for VCN and CN placed near a reactor core, which can significantly increase the neutron emission of the sources into the neutron guides.

3.8. Analytical investigations at the IBR-2 reactor

In 2016, the REGATA facility was used for multi-element instrumental neutron activation analysis of about 3,000 environmental samples (vegetation, soil, air filters), a number of technological, biological and archaeological samples, as well as of samples of extraterrestrial origin. Investigations of test samples were conducted for an interlaboratory comparison of the results under the IAEA program.

4. THE IBR-2 PULSED REACTOR

In 2016, the IBR-2 research nuclear facility was operated in a nominal on-power mode under Rostekhnadzor license № valid until 30.09.2022.

Statistical data on the IBR-2 operation of IBR-2 for physics experiments are presented in Table.

№ cycle	Period	Moderator type	Reactor operation for physics experiments, hr
1	18.01-29.01	water	262
2	08.02-19.02	water	262
3	14.03-28.03	water	328
4	04.04-18.04	water	328
5	16.05-27.05	water	120

№ cycle	Period	Moderator type	Reactor operation for physics experiments, hr
6	26.09-07.10	canceled due to technical reasons	
7	17.10-03.11	water	408
8	15.11-25.11	cryogenic	237
9	05.12-26.12	water	502
Total:			2447

5. NOVEL DEVELOPMENT AND CONSTRUCTION OF EQUIPMENT FOR THE SPECTROMETER COMPLEX OF THE IBR-2 FACILITY

The following major activities were carried out in 2016 in the framework of the project “Development of PTH sample environment system for the DN-12 diffractometer at the IBR-2 facility”:

- a cryostat for a superconducting magnet with HTSC current leads and a cryostat for a high-pressure cell were manufactured;
- a machine for HTSC tape winding was manufactured;
- magnet windings were produced;
- thermal measurements were carried out for both cryostats with a prototype of the magnet in a vertical position with a zero current;
- equipment and materials required for final assembling and commissioning of the PTH system were purchased.

The achieved terminal temperatures of the magnet prototype (13 K), warm ends of HTSC current leads (55-57 K), and sample (2.8 K) correspond to the design values.

6. CONFERENCES AND MEETINGS

1. The 29th Task Force Meeting of the ICP Vegetation organized by The Frank Laboratory of Neutron Physics, Dubna, Russia together with the ICP Vegetation Programme Coordination Centre for Ecology & Hydrology - Bangor, UK 29.02-05.03.2016, Dubna (<http://indico-new.jinr.ru/conferenceDisplay.py?confId=72>).

2. The 24th International Seminar on Interaction of Neutrons with Nuclei: Fundamental Interactions & Neutrons, Nuclear Structure, Ultracold Neutrons, Related Topics (ISINN-24) dedicated to the 60th anniversary of JINR; 24 – 27.05.2016, Dubna. (<http://isinn.jinr.ru>).

3. III International Conference on Small Angle Neutron Scattering (YuMO2016) dedicated to the 80th anniversary of Yuriy Mechislavovich Ostanevich; 6-9.06.2016, Dubna (<http://yumo.jinr.ru/2016>).

4. The Student Training Course: «Advanced Materials Investigation by Means of Neutron Scattering Methods» organized by the Joint Institute for Nuclear Research together with the West University of Timisoara and University Ovidius from Constanta (Romania) 27.08-04.09.2016, Dubna.

5. Workshop on small-angle neutron scattering MURomets 2016; 28-30.09.2016; Gatchina. With the financial and organizational support of the FLNP JINR (<https://oiks.pnpi.spb.ru/events/muromets2016>).

6. The VII International School for Young Scientists and Students “Instruments and Methods of Experimental Nuclear Physics. Electronics and Automatics of Experimental Facilities”; 07-11.11.2016, Dubna (<http://d-instruments.ru/>).
7. Meetings of TANGRA project organized by FLNP JINR and LLC “Diamant”, 20.10.2016, 8-9.12.2016, Dubna.

REFERENCES:

- [1] S.V.Ovsyannikov, M.Bykov, E.Bykova, D.P.Kozlenko, A.A.Tsirlin, A.E.Karkin, V.V.Shchennikov, S.E.Kichanov, H.Gou, A.M. Abakumov, R.Egoavil, J.Verbeeck, C.McCammon, V.Dyadkin, D.Chernyshov, S. van Smaalen, and L.S. Dubrovinsky “Charge ordering transition in iron oxide Fe_4O_5 , involving competing dimer and trimer formation”, *Nature Chemistry*, v. 8, p. 501 (2016).
- [2] N.T.Dang, D.P.Kozlenko, T.L.Phan, S.E.Kichanov, L.H.Khiem, S.H.Jabarov, T.A.Tran, N.V.Dang, T.D.Thanh, D.B.Vo, B.N.Savenko “Structural Polymorphism of Mn-Doped BaTiO_3 ” *Journal of Electronic Materials*, 45, 2477-2483 (2016).
- [3] D.P.Kozlenko, N.T.Dang, T.L.Phan, S.E.Kichanov, N.V.Dang, T.D.Thanh, L.H.Khiem, S.H.Jabarov, T.A.Tran, T.V.Manh, A.T.Le, B.N.Savenko “The Structural, Magnetic and Vibrational Properties of Ti-doped BaMnO_3 ” *Journal of Alloys and Compounds*, accepted (2016).
- [4] S.Ya. Istomin, V.V. Chernova, E.V. Antipov, M.V. Lobanov, I.A. Bobrikov, V.Yu. Yushankhai, A.M. Balagurov, K.Y. Hsu, J.-Y. Lin, J.M. Chen, J.F. Lee, O.S. Volkova, A.N. Vasiliev “Wide range tuning of Mo oxidation state in $\text{La}_{1-x}\text{Sr}_x\text{Fe}_{2/3}\text{Mo}_{1/3}\text{O}_3$ perovskites” *European Journal of Inorganic Chemistry*, v. 2016 (18), pp. 2942-2951 (2016).
- [5] А.М. Балагуров, И.А. Бобриков, Б. Мухаметулы, С.В. Сумников, И.С. Головин “Когерентное кластерное упорядочение атомов в интерметаллиде Fe-27Al” *Письма в ЖЭТФ*, 104(8), 560-567 (2016).
- [6] M.Kubovcikova, Gapon I.V., Zavisova V., Koneracka M., Petrenko V.I., Soltwedel O., Almasy L., Avdeev M.V., Kopcansky P. On the adsorption properties of magnetic fluids: impact of bulk structure. *JMMM*, 2016, in press.
- [7] A.V.Nagornyi, Petrenko V.I., Avdeev M.V., Yelenich O.V., Solopan S.O., Belous A.G., Gruzinov A.Yu., Ivankov O.I., Bulavin L.A. Structural aspects of magnetic fluid stabilization in aqueous agarose solutions. *JMMM*, 2016, in press.
- [8] Yu.I.Prylutskiy, Cherepanov V.V., Kostjukov V.V., Evstigneev M.P., Kyzyma O.A., Bulavin L.A., Ivankov O., Davidenko N.A. and Ritter U. Study of the complexation between Landomycin A and C60 fullerene in aqueous solution. *RSC Adv.*, 2016, V. 6, pp. 81231-81236.
- [9] S.Prylutska, Panchuk R., Goluński G., Skivka L., Prylutskiy Yu., Hurmach V., Skorokhyd N., Borowik A., Wozniowiczka A., Piosik J., Kyzyma O., Haramus V., Bulavin L., Evstigneev M., Buchelnikov A., Stoika R., Berger W., Ritter U., Scharff P. C60 fullerene enhances cisplatin anticancer activity and overcomes tumor cells drug resistance. *Nano Res.*, 2016, accepted
- [10] M.V.Avdeev, Rulev A.A., Bodnarchuk V.I., Ushakova E.E., Petrenko V.I., Gapon I.V., Tomchuk O.V., Matveev V.A., Pleshanov N.A., Kataev E.Yu., Yashina L.V., Itkis D.M. Monitoring of Lithium Plating by Neutron Reflectometry. *Applied Surface Science*, 2016, submitted.
- [11] I.M.Byvshev, Vangeli, I. M., Murugova, T. N., Ivankov, O. O., Kuklin, A. I., Popov, V. I., Yaguzhinsky, L. S. On the existence of two states of OXPHOS system supercomplex in heart mitochondria. *Biochimica et Biophysica Acta - Bioenergetics*, 1857, e35-e36 (2016).
- [12] R.Kepler, Stipp, M., Behrmann, J.H., Ullemeyer, K. & Heidelbach, F. Deformation inside a paleosubduction channel – Insights from microstructures and crystallographic preferred orientations of eclogites and metasediments from the Tauern Window, Austria. *J. Struct. Geol.* 82, 60-79 (2016).
- [13] D. Nikolayev, & Lychagina, T., Zisman, A.A. & Yashina, E. Directly verifiable neutron diffraction technique to determine retained austenite in steel. *Materials Science and Engineering A.*, submitted (2016).
- [14] Ch.Scheffzük, Müller, B.I.R., Breuer, S., Altangerel B. & Schilling, F.R. Applied Strain Investigation on Sandstone Samples Using Neutron Time-of-Flight Diffraction at the Strain Diffractometer EPSILON, IBR-2M Dubna. *Mongolian J. Physics*, submitted (2016).
- [15] S.Breuer, Schilling, F.R., Scheffzük, Ch. & Müller, B.I.R. Forward Modeling Neutron Time-of-Flight Diffraction Data for Uniaxial Load Conditions by Using the Example of Sandstone. *J. Appl. Cryst.*, submitted (2016).